Author(s): Ge, Z.; Eronen, T.; de Roubin, A.; Ramalho, M.; Kostensalo, J.; Kotila, J.; Suhonen, J.; Nesterenko, D. A.; Kankainen, A.; Ascher, P.; Beliuskina, O.; Flayol, M.; Gerbaux, M.; Grévy, S.; Hukkanen, M.; Husson, A.; Jaries, A.; Jokinen, A.; Moore, I. D.; Pirinen, P.; Romero, J.; Stryjczyk, M.; Virtanen, V.; Zadvornaya, A.

Title: β− decay Q-value measurement of 136Cs and its implications for neutrino studies

Year: 2023

Version: Published version

β^- decay Q-value measurement of ^{136}Cs and its implications for neutrino studies

Z. Ge,[1,2,*] T. Eronen,[2,†] A. de Roubin,[3,‡] M. Ramalho,[2] J. Kostensalo,[4] J. Kotila,[2,5,6] J. Suhonen,[2,§] D. A. Nesterenko,[2] A. Kankainen,[2] P. Ascher,[3] O. Beliuskina,[2] M. Flayol,[3] M. Gerbaux,[3] S. Grévy,[3] M. Hukkanen,[2,3] A. Husson,[3] A. Jaries,[2] A. Jokinen,[2] I. D. Moore,[2] P. Pirinen,[2] J. Romero,[2,7] M. Stryjczyk,[2] V. Virtanen,[2] and A. Zadvornaya[2,‖]

[1]*GSI Helmholtzzentrum für Schwerionenforschung GmbH, 64291 Darmstadt, Germany*
[2]*Department of Physics, University of Jyväskylä, P.O. Box 35, FI-40014, Jyväskylä, Finland*
[3]*Université de Bordeaux, CNRS/IN2P3, LP2I Bordeaux, UMR 5797, F-33170 Gradignan, France*
[4]*Natural Resources Institute Finland, Yliopistokatu 6B, FI-80100, Joensuu, Finland*
[5]*Finnish Institute for Educational Research, University of Jyväskylä, P.O. Box 35, FI-40014, Jyväskylä, Finland*
[6]*Center for Theoretical Physics, Sloane Physics Laboratory, Yale University, New Haven, Connecticut 06520-8120, USA*
[7]*Department of Physics, University of Liverpool, Liverpool L69 7ZE, United Kingdom*

(Received 7 June 2023; accepted 19 September 2023; published 11 October 2023)

The β^- decay Q value of ^{136}Cs ($J^\pi = 5^+$, $t_{1/2} \approx 13$ d) was measured with the JYFLTRAP Penning trap setup at the Ion Guide Isotope Separator On-Line facility of the University of Jyväskylä, Finland. The monoisotopic samples required in the measurements were prepared with a new scheme utilized for the cleaning, based on the coupling of dipolar excitation with Ramsey's method of time-separated oscillatory fields and the phase-imaging ion-cyclotron-resonance technique. The Q value is determined to be 2536.83(45) keV, which is ≈4 times more precise and 11.4(20) keV (≈6σ) smaller than the adopted value in the most recent Atomic Mass Evaluation AME2020. The daughter, ^{136}Ba, has a 4^+ state at 2544.481(24) keV and a 3^- state at 2532.653(23) keV, both of which can potentially be ultralow Q-value end states for the ^{136}Cs decay. With our new ground-to-ground state Q value, the decay energies to these two states become −7.65(45) keV and 4.18(45) keV, respectively. The former is confirmed to be negative at the level of ≈17σ, which verifies that this transition is not a suitable candidate for neutrino mass determination. On the other hand, the slightly negative Q value makes this transition an interesting candidate for the study of virtual β-γ transitions. The decay to the 3^- state is validated to have a positive low Q value which makes it a viable candidate for neutrino mass determination. For this transition, we obtained a shell-model-based half-life estimate of $2.1^{+1.6}_{-0.8} \times 10^{12}$ yr. Furthermore, the newly determined low reaction threshold of 79.08(54) keV for the charged-current $\nu_e + {}^{136}\mathrm{Xe}\ (0^+) \rightarrow {}^{136}\mathrm{Cs}^* + e^-$ neutrino capture process is used to update the cross sections for a set of neutrino energies relevant to solar ^{7}Be, pep, and CNO neutrinos. Based on our shell-model calculations, the new lower threshold shows event rates of 2–4 percent higher than the old threshold for several final states reached by the different species of solar neutrinos.

DOI: 10.1103/PhysRevC.108.045502

I. INTRODUCTION

The standard model (SM) predicts that the neutrino is massless, and how neutrinos acquire their small masses, verified by the neutrino-oscillation experiments, is consequently a matter of great theoretical interest and may be evidence of new physics beyond the SM [1–3]. Assessing the neutrino mass scale has been an outstanding task for particle physics, as the absolute value of the neutrino mass would provide an important parameter to extend the SM of particle physics and to understand the origin of fermion masses beyond the Higgs mechanism. The neutrinoless double β decay experiments aim to probe if neutrinos are of Dirac or Majorana nature and to measure the effective Majorana neutrino mass [4–6]. This method is, however, nuclear-model dependent and strongly relies on the calculation of the involved nuclear matrix elements, sensitive to the details of the nuclear wave functions describing the initial, intermediate, and final nuclear states of the process [6]. Complementary ways to probe the involved wave functions have been devised, like the nuclear muon capture, charge-exchange, and double charge-exchange reactions [6]. Nevertheless, β^--decay or electron-capture (EC) spectrum end-point study remains currently the only laboratory method to provide a model-independent measurement of the absolute scale of the (anti)neutrino mass. In these experiments the most sensitive upper limits on the mass of the electron neutrino m_{ν_e} have been achieved by investigating the end point of the β^- electron spectrum. The most stringent upper limit of 0.8 eV/c^2 [90% confidence level (C.L.)] for the

*Corresponding author: z.ge@gsi.de
†Corresponding author: tommi.eronen@jyu.fi
‡Present address: KU Leuven, Instituut voor Kern- en Stralingsfysica, B-3001 Leuven, Belgium.
§Corresponding author: jouni.t.suhonen@jyu.fi
‖Present address: II. Physikalisches Institut, Justus-Liebig-Universität Gießen, 35392 Gießen, Germany.

electron-antineutrino mass is obtained by studying the tritium decay in the KATRIN (KArlsruhe TRitium Neutrino) experiment [7], and an upper limit of 150 eV/c^2 (95% C.L.) is obtained for the electron-neutrino mass, as achieved by studying the EC of ^{163}Ho in the ECHo experiment [8]. In these decay experiments, as small as possible Q value of the decay is essential to partially balance the limitation on the statistics when looking for the tiny (anti)neutrino-mass generated distortion close to the end-point energy [9,10]. For the β-decay experiments the fraction of decays in a given energy interval ΔE below the end-point Q value is proportional to $(\Delta E/Q)^3$, whereas for the EC this dependence on the Q value can be even more drastic especially in the case when the Q value is close to an atomic excitation level [11,12]. The preference for lower Q values is based on the fact that the fraction of decays in a given energy interval ΔE below the end-point will be increased with a lower Q value.

Up to now, only ground-state–to–ground-state (gs-to-gs) decay cases of ^{3}H, ^{187}Re (β^- decay), and ^{163}Ho (electron capture), having the lowest known gs-to-gs Q values, have been used for direct neutrino-mass-determination experiments. The β^- decay of tritium, $^3\mathrm{H}(1/2^+) \rightarrow {}^3\mathrm{He}(1/2^+)$, which is of the allowed type (a Fermi and/or Gamow-Teller transition) with a Q value ($Q^0_{\beta^-}$) of ≈18.6 keV [13], is utilized to measure the effective electron antineutrino mass. In an EC transition, like $^{163}_{67}\mathrm{Ho} + e^- \rightarrow {}^{163}_{66}\mathrm{Dy}^* + \nu_e$, one can determine the effective electron neutrino mass from the analysis of the endpoint region of the excitation energy spectrum of the daughter atom ^{163}Dy, whose Q_{EC} is ≈2.8 keV.

The possibility to utilize transitions to excited final states has recently attracted a lot of attention, as reviewed in [14]. Intensive search for isotopes featuring β^-/EC transitions from ground-state–to–excited-states (gs-to-es) with a positive low Q value, preferably ultralow (<1 keV), has recently been carried out [11,12,15–24]. From the technology point of view, suitable detectors are available as described in [25]. It is imperative to search for nuclides that could be used for competitive experiments using gs-to-es decays. In addition to the slightly positive Q values, the slightly negative Q values can also be of interest in seeking for a new type of transition process, like the virtual radiative "detour" transitions (RDT). A recent study of this type of transition in ^{59}Ni was carried out in Ref. [26,27], where a virtual transition via a state 26 keV higher than allowed by the Q value of the transition was found to contribute about 4% to the experimental gamma spectrum. This result highlights that a slightly energetically forbidden transition will open a door to the possibility to study RDTs. Since the probability of such a detour transition is proportional to $(E^* - E_\gamma)^{-2}$ [26], where E_γ is the energy of the emitted gamma ray, a transition with an ultra-low negative Q value would make the RDT a relatively strong channel and thus easier to detect.

Special attention is given to possible alterations in neutrino-capture cross sections of low-energy neutrinos, for example those from the sun, by the more precise Q-value measurements. Of interest are the charged-current $\nu_e + {}^{136}\mathrm{Xe}$ $(0^+) \rightarrow {}^{136}\mathrm{Cs}^* + e^-$ neutrino-capture cross sections for the solar ^{7}Be, pep, and CNO neutrinos where our improved threshold value could alter the cross sections and thus the detection potential of these neutrinos in xenon-based solar-neutrino observatories [28].

In summary, a precise and accurate determination of the transition Q value is extremely important to validate the possible further usage of low Q-value-decay candidate transitions in the context of searches for the absolute (anti)neutrino mass scale or for radiative "detour" transitions. Also implications for the low-energy solar-neutrino detection could potentially be of relevance. The allowed transition ^{136}Cs (5^+, $t_{1/2} \approx 13$ d) $\rightarrow$ ^{136}Ba* (4^+, 2544.481(24) keV [29–32]), is of paramount interest for the antineutrino-mass studies because of its small gs-to-es Q value $Q^*_{\beta^-}$ ($= Q^0_{\beta^-} - E^*$) of 3.7(19) keV [33]. This transition is proposed to be one of the most promising candidates for neutrino mass determination [24]. The $Q^*_{\beta^-}$ value for this transition can be deduced from the sub-keV-precision energy-level E^* data in [32] and the gs-to-gs Q value of 2548.2(19) keV from AME2020 [33]. The gs-to-gs Q value of ^{136}Cs in AME2020 is evaluated primarily using data from two $^{136}\mathrm{Cs}(\beta^-)\,^{136}$Ba-decay experiments performed more than 60 years ago [34,35]. Previous studies have already demonstrated that Q values derived in indirect methods, such as decay spectroscopy, show large discrepancies with those from direct mass measurements and can be inaccurate over a wide range of mass numbers [20,36,37]. The AME2020 Q value with its large uncertainty of 1.9 keV, and its possible inaccuracy, requires verification to unambiguously identify energetically allowed or forbidden low-Q transitions. To confirm whether there are β^--decay transitions from ^{136}Cs that can serve as potential candidates for future antineutrino-mass determination experiments or be eligible for studies of RDTs, the gs-to-gs Q value needs to be measured directly with a sub-keV uncertainty.

Penning trap mass spectrometry (PTMS) is the leading technique for accurate and precise mass and Q-value determination. It relies on the determination of the cyclotron frequency ratio of parent and daughter ions, from which the mass difference can be extracted. In this article, we report on the first-time direct determination of the gs-to-gs β^--decay Q value of ^{136}Cs with the JYFLTRAP PTMS. A method based on utilization of a dipolar radiofrequency (RF) excitation of ion motion with time-separated oscillatory fields in the precision trap coupled with the phase-imaging ion-cyclotron-resonance (PI-ICR) technique, is used to prepare monoisotopic ions to ensure a contaminant-free high-precision Q-value determination. The new scheme allows for an efficient isobaric ion separation of ^{136}Cs from the small mass-difference (90 keV/c^2) contaminant of ^{136}Xe, and isomeric ion separation of ^{136}Cs from its co-produced low-lying isomeric state ($t_{1/2} \approx 17.5$ s) at 518 keV.

II. EXPERIMENTAL METHOD

The measurement was performed at the Ion Guide Isotope Separator On-Line facility (IGISOL) [38] with the JYFLTRAP double Penning trap mass spectrometer [39,40] at the University of Jyväskylä, Finland. A schematic view of the experimental setup is shown in Fig. 1. The two ion species of the decay pair, ^{136}Cs and ^{136}Ba, were produced by irradiating a natural uranium target foil with a few μA proton

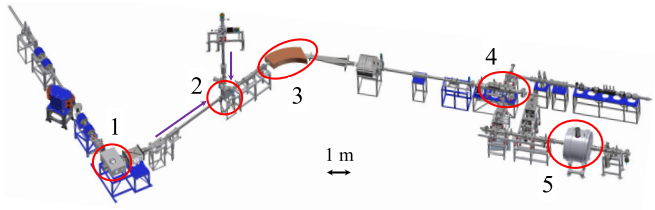

FIG. 1. Schematic view of the IGISOL facility. The $^{136}Cs^+$ and $^{136}Ba^+$ ions were produced with proton-induced fission reactions on a natural uranium target within the IGISOL target chamber (1). The online beam was selected with an electrostatic kicker (2) and the dipole magnet (3) was used to transport only ions with $A/q = 136$. The ion cooling and bunching was carried out in the RFQ cooler-buncher (4) and the final Q value and mass measurement was performed with the JYFLTRAP Penning trap setup (5).

beam at 30 MeV from the K-130 cyclotron. The produced ions were stopped and thermalized in a helium-filled gas cell, and extracted out with the gas flow and electric fields via a sextupole ion guide [40]. The extracted ions were accelerated to 30 keV of energy and transported further to the 55° dipole magnet having a mass resolving power of $M/\Delta M \approx 500$. This allows isobaric separation to select only ions with $A/q = 136$, including ^{136}Cs, ^{136m}Cs, ^{136}Xe, ^{136}Ba, ^{136}Te, and ^{136}I that are all produced in the fission reaction. The ions are then delivered to a radiofrequency quadrupole cooler-buncher [41], where they are accumulated, cooled and bunched prior to sending the bunches to the JYFLTRAP double Penning trap mass spectrometer for further purification and the final mass-difference measurements.

JYFLTRAP consists of two cylindrical Penning traps in a 7 T magnetic field. The first trap (purification trap) is filled with helium buffer gas and is used for isobaric purification via the buffer-gas cooling technique [45]. This technique can provide a mass purification with a resolving power of around 10^5. For higher mass resolving power, the Ramsey cleaning method [42] can be employed. Figure 2 shows the schematic diagram of the steps employed prior to the actual mass and Q-value measurements in the second trap (precision trap).

In this experiment, a purified sample of decay-daughter ions $^{136}Ba^+$ was prepared with the buffer-gas cooling technique, which was enough to remove all other ion species. This is shown in Fig. 3, where the mass-sensitive quadrupole excitation frequency was scanned over the resonance frequencies of the $A/q = 136$ ion species.

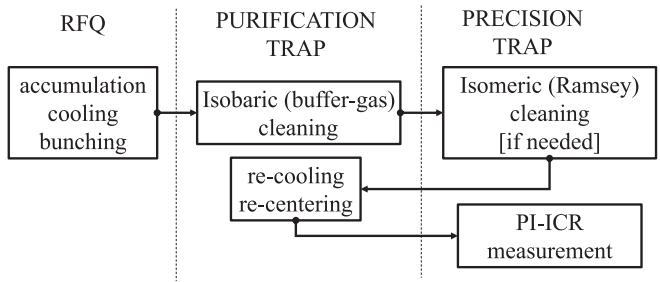

FIG. 2. Schematic of the measurement cycle at JYFLTRAP [39,42–44]. The purification trap is used for isobaric cleaning, and it is often sufficient to provide contaminant-free samples in most of the cases studied. The precision trap is used for further isomeric cleaning when higher resolving power is needed and final high-precision mass or Q-value measurements.

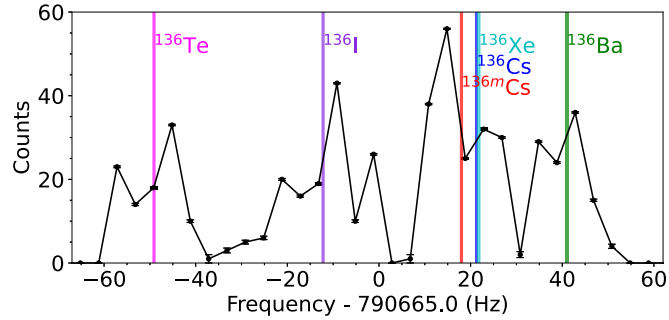

FIG. 3. Detected number of ions downstream from the PTMS as a function of quadrupole excitation frequency in the purification trap. The vertical lines in various colors indicate the excitation frequency to be applied for the selection of the corresponding ion species of singly charged ions of mass $A = 136$.

For the preparation of clean samples of $^{136}Cs^+$ decay-parent ions, higher resolving power is needed. As indicated in Fig. 3, the selection frequencies to center ions of ^{136}Cs, ^{136m}Cs, ^{136}Xe are too close to completely separate them from each other. In this case, the Ramsey cleaning technique [42] is employed right after the sideband buffer-gas cooling. Due to the closeness in mass of $^{136}Cs^+$ to both $^{136m}Cs^+$ and $^{136}Xe^+$, it is still challenging by the use of the conventional Ramsey cleaning technique [42] to completely purify the ion sample of $^{136}Cs^+$. Here, we introduce a new cleaning scheme, which relies on scanning the dipolar excitation (so-called cleaning excitation) frequency over the ν_+ frequency of the ion species present in the precision trap while applying the phase-imaging ion-cyclotron-resonance (PI-ICR) technique [43,44] to identify which ions are ultimately transmitted.

The dipolar excitation was applied as two 22-ms fringes interrupted for 762 ms. Depending on the applied frequency, the ions are left with different cyclotron motion amplitude. If this amplitude is high enough, the ions will hit the electrode of the diaphragm between the two traps in the subsequent transfer back to the first trap for recooling and centering. To assess the composition of the remaining ion bunch, the ions are transferred again to the precision trap where the PI-ICR method is utilized.

The phase accumulation time in the PI-ICR identification was chosen to be 458 ms. This allowed sufficient angular separation to unambiguously observe all three ion species. Figure 4 shows the dipolar excitation scan while gating on the well-resolved spots of different species. Setting the excitation frequency to maximally transmit $^{136}Cs^+$ ions, the other two are, if not completely, at least heavily suppressed (contamination ratio of less than 2%). After the verification, the cleaning settings are locked and the final mass measurement with the PI-ICR technique commenced. The actual PI-ICR mass measurement was performed with phase accumulation times chosen such that the spots of different ions did not overlap and thus interfere with spot position fitting.

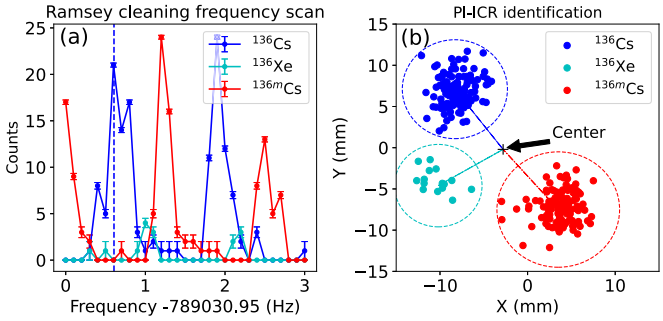

FIG. 4. (a) Ramsey-type dipole excitation frequency scan with a 22 ms (On) - 762 ms (Off) - 22 ms (On) excitation pattern in the second trap filtered by the positional gates shown in (b) using the PI-ICR identification (458 ms phase accumulation time) plot. The used angular gates are highlighted. The vertical dashed line shows the chosen optimal frequency to transmit ^{136}Cs ions while suppressing the others.

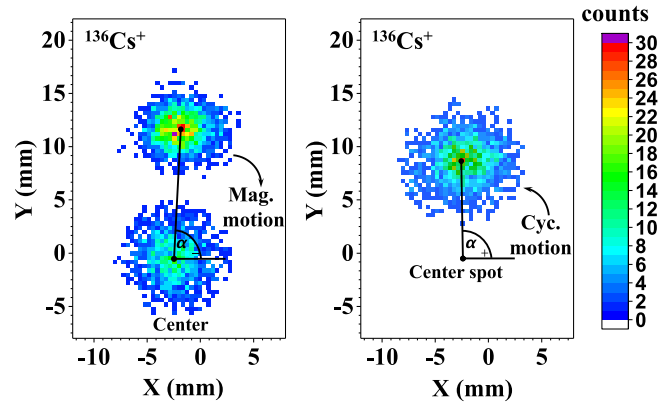

FIG. 5. ^{136}Cs$^+$ ion spots of center, cyclotron phase and magnetron phase on the two-dimensional position-sensitive MCP detector after a PI-ICR excitation pattern with an accumulation time of 458 ms. The magnetron phase spot along with a center spot is illustrated on the left and the cyclotron phase spot on the right. The cyclotron frequency ν_c is deduced from angle difference between the two spots relative to the center spot. The color bar indicates the number of detected ions for each pixel.

The PI-ICR technique used in this work for the Q value measurement is the state-of-the-art Penning trap mass measurement technique for short-lived ions [43,46,47]. This technique allows extraction of the free-space ion-cyclotron frequency

$$\nu_c = \frac{1}{2\pi}\frac{q}{m}B, \tag{1}$$

where q is the charge of the ion, m the mass, and B the magnetic field of the trap, through observation of the final motional phase of the ions. The measurement begins by initial excitation of cyclotron motion of the ions with a short ($\approx$1 ms) dipolar pulse at the ν_+ frequency. This is followed by a cyclotron-to-magnetron motion quadrupolar conversion pulse at frequency ν_c. Finally, ions are extracted from the trap to be detected with the position-sensitive MCP detector.

The quadrupolar conversion pulse needs to be applied with two different delay times while keeping the overall cycle identical. One short delay is used to record the so-called magnetron phase and the other, longer, for the cyclotron phase. The delay difference of these settings define the phase-accumulation time t_{acc}. The cycle is described in detail in [43,44]. The phase angle detected between the two cycles with respect to the center spot is $\alpha_c = \alpha_+ - \alpha_-$, where α_+ and α_- are the polar angles of the cyclotron and magnetron motion phases. The cyclotron frequency ν_c is derived from

$$\nu_c = \frac{\alpha_c + 2\pi n_c}{2\pi t_{acc}}, \tag{2}$$

where n_c is the number of complete revolutions of the measured ions during the phase accumulation time t_{acc}. Two different accumulation times, 458 ms and 428 ms, were used in this measurement. These times were chosen to ensure contaminant ions (especially ^{136m}Cs and ^{136}Xe for ^{136}Cs frequency determination) do not appear on the same angle with the ion of interest in case of leakage from the trap.

The excitation time was fine-tuned to be multiple integers of ν_c period such that the angle α_c did not exceed a few degrees. This reduces the shift in the ν_c measurement due to the conversion of the cyclotron motion to magnetron motion and the possible distortion of the ion-motion projection onto the detector to a level well below 10^{-10} [46]. Additionally, the start time of the initial cyclotron motion excitation was scanned over one magnetron period and the extraction delay was varied over one cyclotron period to account for any residual magnetron and cyclotron motion that could shift the different spots. An example of phase spots collected is shown in Fig. 5. In total, $\approx$13 h of data was collected in interleaved ν_c measurements of ^{136}Cs$^+$ and ^{136}Ba$^+$ ions.

The Q_{β^-} value can be derived using the cyclotron frequency ratio of the measured ion pair:

$$Q_{\beta^-} = (M_p - M_d)c^2 = (R-1)(M_d - qm_e)c^2 + (R\cdot B_d - B_p), \tag{3}$$

where M_p and M_d are the masses of the parent (^{136}Cs$^+$) and daughter (^{136}Ba$^+$) atoms, respectively, and R their cyclotron frequency ratio ($\frac{\nu_{c,d}}{\nu_{c,m}}$) for singly charged ions ($q = 1$). m_e is the mass of an electron. B_p and B_d are the electron binding energies of the parent and daughter atoms, which are neglected as it is on the order of a few eV [48] and R is off from unity by less than 10^{-4}. Since both the parent and daughter have the same A/q, mass-dependent shifts effectively become inferior compared to the statistical uncertainty achieved in the measurements. Moreover, due to the very small relative mass difference of the parent and daughter ($\Delta M/M < 10^{-4}$), the contribution of the uncertainty to the Q value from the mass uncertainty of the reference (daughter), 0.24 keV/c^2, can be neglected.

III. RESULTS AND DISCUSSION

In total, 13.5 h of PI-ICR measurement data with two different accumulation times were recorded. The full sequence, consisting of measurement of magnetron phase, cyclotron phase, and center spots required about 3 min to complete.

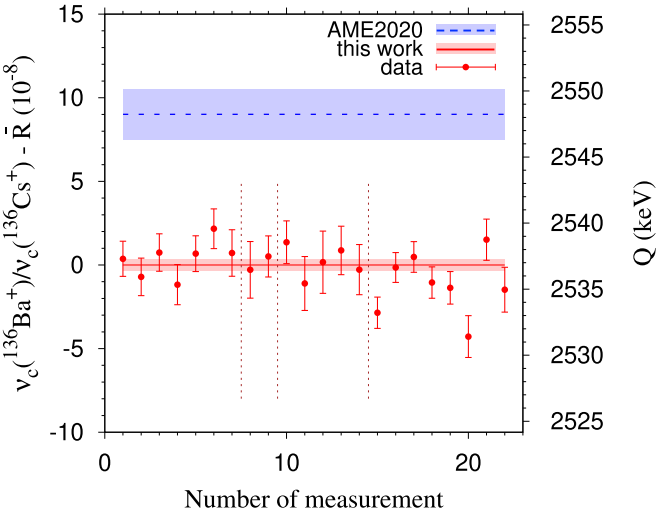

FIG. 6. The deviation (left axis) of the individually measured cyclotron frequency ratios R [$\nu_c(^{136}Ba^+)/\nu_c(^{136}Cs^+)$] from the measured value $\overline{R}$ and (right axis) Q values in this work compared to value adopted from AME2020 [33,52]. The red points with uncertainties are measured individual data collected in four different time slots, which are separated with vertical brown dashed lines. The weighted average value from this work $\overline{R} = 1.000\,020\,039\,1(35)$ is illustrated by the horizontal solid red line with its 1σ uncertainty band. The dashed blue line is the value in AME2020 with its 1σ uncertainty area shaded in blue.

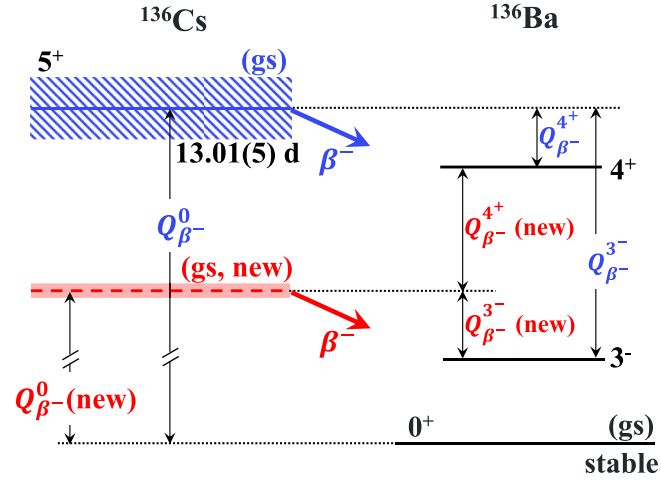

FIG. 7. Partial decay diagram for the ^{136}Cs ground state to ground state and possible ultralow Q-value excited states of 4^+ and 3^- in ^{136}Ba using Q values from AME2020 [33,52] in comparison to this work. The levels drawn with solid lines show the excited states with the Q values from AME2020 and dashed lines from the refined Q values in this work (new). The hatched and shaded areas (in blue for the 3^- and in red for the 4^+ state) illustrate the corresponding 1σ uncertainty in the Q values. Table II lists the Q values in detail.

This was sequentially repeated for both ion species $^{136}Cs^+$ and $^{136}Ba^+$. In the analysis, the position of each spot was fitted with the maximum-likelihood method. A few rounds were summed to have a few tens of detected ions for fitting. The phase angles were calculated accordingly based on the determined positions of the phases to deduce the ν_c frequency of each ion species. The ν_c of the daughter $^{136}Ba^+$ as a reference was linearly interpolated to the time of the measurement of the parent $^{136}Cs^+$ to deduce the cyclotron frequency ratio R. Ion bunches containing no more than five detected ions were considered in the data analysis in order to reduce a possible cyclotron frequency shift due to ion-ion interactions [49,50]. The count-rate related frequency shifts were not observed in the analysis. The temporal fluctuation of the magnetic field has been measured to be $\delta_B(\nu_c)/\nu_c = \Delta t \times 2.01(25) \times 10^{-12}$ min [44], where Δt is the time interval between two consecutive reference measurements. Contribution of temporal fluctuations of the magnetic field to the final frequency ratio uncertainty was less than 10^{-10}. The frequency shifts in the PI-ICR measurement due to ion image distortions, which were well below the statistical uncertainty, were ignored in the calculation of the final uncertainty. The weighted mean ratio $\overline{R}$ of all single ratios was calculated along with the inner and outer errors to deduce the Birge ratio [51]. The maximum of the inner and outer errors was taken as the weight to calculate $\overline{R}$. The determination of Q_{β^-} from $\overline{R}$ depends on the measured cyclotron frequency ν_c via Eq. (3). In Fig. 6, results of the analysis including all data with comparison to literature values are demonstrated. The final frequency ratio $\overline{R}$ with its uncertainty as well as the corresponding Q value are $\overline{R} = 1.000\,020\,039\,1(35)$ and $Q_{\beta^-} = 2536.83(45)$ keV, respectively.

A comparison of our results with the literature values is tabulated in Table I. The mass excess of the parent nucleus ^{136}Cs (5^+) was deduced to be $-86350.09(54)$ keV. The gs-to-gs Q value ($Q^0_{\beta^-}$), determined to be 2536.83(45) keV from this work, is ≈ 4 times more precise than that derived from the evaluated masses in AME2020 [33,52]. The new $Q^0_{\beta^-}$ value has a deviation of $-11.4(20)$ keV from the AME2020 value and is $\approx 6\sigma$ smaller. The high-precision β^- decay energy from this work, together with the nuclear energy level data from [32] of the excited states of ^{136}Ba as tabulated in Table II, were used to determine gs-to-es Q value ($Q^*_{\beta^-}$) of these two states, see Fig 7. The calculated Q values of potential candidate transitions of the ground state of parent nuclei ^{136}Cs to the excited states of daughter ^{136}Ba are tabulated in Table II. Our results confirm that the decay of the ground state of ^{136}Cs to the 4^+ excited state in ^{136}Ba with an excitation energy of 2544.481(24) keV is energetically forbidden. The Q_{β^-} value is negative with $\approx 17\sigma$ confidence. The decay channel to the 3^- excited state at 2532.653(23) keV, having a refined Q value of 4.18(45) keV, is energetically allowed and serves as a possible low Q-value transition to be used for neutrino-mass determination. The unexpectedly large deviation of the $Q^0_{\beta^-}$, which lowers the gs-to-es Q value of 15.5(19) keV by more than 10 keV for the excited state of 2532.653(23) keV, makes the decay to this state of considerable interest.

The partial half-life of the transition, which is of first-forbidden unique type, can be estimated with a microscopic nuclear model. It depends on the Q value through a phase-space factor and on nuclear structure through the involved nuclear matrix element (NME). The relevant NME was calculated using the nuclear shell model in the full $0g_{9/2}-$

TABLE I. Mean cyclotron frequency ratio $\overline{R}$ between the daughter ^{136}Ba (0^+) and parent ^{136}Cs (5^+) nuclei, Q_{β^-} values (in keV) and the mass excess (in keV/c^2) of parent nuclei determined in this work in comparison with the AME2020 values [33].

	$\overline{R}$	Q_{β^-}	mass excess [^{136}Cs (5^+_{gs})]
AME2020		2548.2(19)	−86338.9(19)
This work	1.000 020 039 1(35)	2536.83(45)	−86350.09(54)

$1d - 2s - 0h_{11/2}$ model space using the effective interaction SN100PN [53]. The calculation was carried out using the shell-model code NUSHELLX@MSU [54]. To account for the well-known problem of the shell model, underestimation of the half-lives of β-decay transitions [55], we adopt an effective value of the axial-vector coupling constant $g_A^{\text{eff}} = 1$, while the 1σ uncertainties related to the shell-model calculation are estimated by varying g_A^{eff} between 0.8 and 1.2 (see, e.g., [55]). The phase-space factor was calculated using exact Dirac electron wave functions with finite nuclear size and electron screening as was previously done for double β decays [56] and allowed β decay [21]. The used formalism for calculating phase-space factors for first-forbidden unique transitions was adopted from [57]. The resulting theoretical half-life estimate is $2.1^{+1.6}_{-0.8} \times 10^{12}$ yr. The half-life as a function of Q value is presented in Fig. 8. The best estimate corresponds to a branching ratio of about 1.7×10^{-12}%.

As an isotope which undergoes double β decay, ^{136}Xe is particularly well suited as a target for study of the charged-current (CC) neutrino capture process $\nu_e + {}^{136}\text{Xe}(0^+) \rightarrow {}^{136}\text{Cs}^* + e^-$ [58,59]. It features a low reaction threshold of $Q = 90.3(19)$ keV (mass difference from AME2020 [33,52]) and a relatively large cross section due to the sizable Gamow-Teller transition strengths connecting the 0^+ ^{136}Xe ground state and the lowest-lying 1^+ excited states of ^{136}Cs. The signal generated in the detector is the combination of the outgoing electron and any γ rays or conversion electrons emitted as the Cs nucleus relaxes to its ground state. Recently, many new low-lying states in ^{136}Cs have been identified, several of which are isomeric and potentially can be used in filtering events [60]. As the reaction threshold Q of ^{136}Xe is low enough (lowest among all naturally occurring isotope of xenon), this reaction can be used to search for neutrinos from the solar carbon-nitrogen-oxygen (CNO) cycle [61,62], and can also provide a unique measurement of ^{7}Be neutrinos, which may enable novel measurements of temperature of the solar core [63]. With the mass excess of ^{136}Cs from our measurements combined with the precise mass value of ^{136}Xe measured at FSU Penning trap [33,52,64], we refined the Q value to be 79.1(5) keV. This value is 11.2(19) keV lower than the evaluated value from AME2020, which will increase the solar neutrino capture rates in the CC neutrino capture process. The same final state of ^{136}Cs with a lower Q value will indicate a higher sensitivity to search for CC absorption of MeV-scale fermionic dark matter on nuclei as well [61,65].

The $\nu_e + {}^{136}\text{Xe}(0^+) \rightarrow {}^{136}\text{Cs}^* + e^-$ neutrino capture process to the two lowest-lying 1^+ states of ^{136}Cs has been studied earlier in Ref. [28]. The wave functions of the initial and final states were computed in the nuclear shell model. Here, we update the cross sections with the new Q value for a set of neutrino energies relevant to solar ^{7}Be, pep, and CNO neutrinos. The results are shown in Table III. The new lower threshold will result in event rates roughly two to four percent higher than the old threshold for the given final states and listed species of solar neutrinos.

IV. CONCLUSION

A new scheme of preparing monoisotopic samples of ^{136}Cs and ^{136}Ba, based on the coupling of the Ramsey cleaning method and the PI-ICR technique to enhance the separation capability of JYFLTRAP, has been employed. A direct high-precision gs-to-gs β^- decay Q-value measurement of $^{136}\text{Cs}(5^+) \rightarrow {}^{136}\text{Ba}(0^+)$ was performed using the PI-ICR technique at the JYFLTRAP double Penning trap mass spectrometer. A Q value of 2536.83(45) keV was obtained and its precision is improved by a factor of four. A discrepancy of around 6 standard deviations is found compared to the adopted value in the AME2020. We confirm that one of the two potential ultralow Q-value β^--decay transitions, $^{136}\text{Cs}(5^+) \rightarrow {}^{136}\text{Ba}^*$ [4^+, 2544.481(24) keV], is energetically forbidden at the 17σ level. A new Q value of −7.65(45) keV was measured for this transition. This is more than a factor of three smaller than the Q value of −26 keV for the transition in ^{59}Ni, resulting in 9 times stronger transition probability for the detour transition. While the negative Q values exclude

TABLE II. Potential candidate transitions of initial state of parent nucleus ^{136}Cs (5^+, ground state), to the excited states of daughter ^{136}Ba with ultralow Q values. The first column gives the spin and parity of the excited final state of ^{136}Ba for the low Q-value transition. The second column gives the decay type. The third column gives the derived decay $Q^*_{\beta^-}$ value in units of keV from literature (Lit.) [33] and the fourth column from this work (new). The fifth column gives the experimental excitation energy with the experimental uncertainty [32] in units of keV. The last column shows the confidence (σ) of the Q value being nonzero. A negative value indicates a negative Q value. "1st FU" represents first forbidden unique.

Final state of ^{136}Ba	Decay type	$Q^*_{\beta^-}$ (Lit.)	$Q^*_{\beta^-}$ (new)	E^*	$Q/\delta Q$ (new)
4^+	allowed	3.7(19)	−7.65(45)	2544.481(24)	−17
3^-	1st FU	15.5(19)	4.18(45)	2532.653(23)	9

TABLE III. Total cross sections of the $\nu_e + {}^{136}\mathrm{Xe}(0^+) \rightarrow {}^{136}\mathrm{Cs}^* + e^-$ neutrino capture process for the two lowest-lying 1^+ final states of ^{136}Cs (column 1) with discrete neutrino energies (column 2) in a range relevant to solar ^{7}Be, pep, and CNO neutrinos. Results are shown for the new threshold 79.08 keV (column 3) and the old threshold 90 keV as used in Ref. [28] (column 4). The calculations were made in the nuclear shell model as described in Ref. [28].

Final state	E_ν (MeV)	NEW σ_{tot} (cm^2) ($Q = 79.08$ keV)	OLD σ_{tot} (cm^2) ($Q = 90$ keV)
1_1^+	0.7	1.16×10^{-44}	1.12×10^{-44}
(590 keV)	0.8	1.57×10^{-44}	1.52×10^{-44}
	0.9	2.06×10^{-44}	2.00×10^{-44}
	1.0	2.60×10^{-44}	2.54×10^{-44}
	1.1	3.21×10^{-44}	3.14×10^{-44}
	1.2	3.88×10^{-44}	3.80×10^{-44}
	1.3	4.60×10^{-44}	4.52×10^{-44}
	1.4	5.38×10^{-44}	5.29×10^{-44}
1_2^+	1.0	7.57×10^{-45}	7.32×10^{-45}
(890 keV)	1.1	1.01×10^{-44}	9.82×10^{-45}
	1.2	1.30×10^{-44}	1.27×10^{-44}
	1.3	1.63×10^{-44}	1.59×10^{-44}
	1.4	1.99×10^{-44}	1.95×10^{-44}
	1.5	2.39×10^{-44}	2.34×10^{-44}
	1.6	2.81×10^{-44}	2.76×10^{-44}
	1.7	3.27×10^{-44}	3.22×10^{-44}

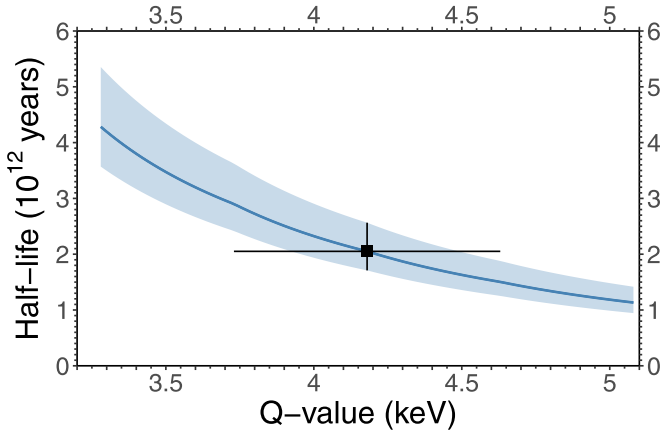

FIG. 8. Theoretical estimate for the partial half-life of the first-forbidden unique transition $^{136}\mathrm{Cs}(5^+_{\mathrm{gs}}) \rightarrow {}^{136}\mathrm{Ba}(3^-)$ with a Q-value of 4.18(45) keV. The shaded area represents a 1σ uncertainty for a given Q value, while the horizontal error bar represents the 1σ uncertainty of the Q value, and the vertical error bar the 1σ nuclear structure uncertainty for the best estimate of the Q value.

the use of this transition to study neutrino mass, the small negative Q values could make it a candidate for the study of β-γ detour transitions proceeding via virtual states. Our results underline the need to measure the Q values to high precision. Not only for the sake of better precision, but, as seen here, existing data can simply be significantly off. For a long-term project building a detector utilizing gs-to-es transitions to measure the mass of a neutrino, it is imperative to know the decay with high accuracy. Moreover, we verify that another transition, ^{136}Cs $(5^+) \rightarrow {}^{136}\mathrm{Ba}^*$ [3^-, 2532.653(23) keV], as a first-forbidden unique transition with a simple universal spectral shape, is positively allowed at a level of 9σ with a small low Q value and thus is a possible candidate for future neutrino mass determination experiment. The refined mass difference of ground states of ^{136}Xe and ^{136}Cs indicates a higher sensitivity of ^{136}Xe as a target for study of charged-current (CC) neutrino capture processes.

ACKNOWLEDGMENTS

We acknowledge the staff of the Accelerator Laboratory of University of Jyväskylä (JYFL-ACCLAB) for providing stable online beam. We thank the support by the Academy of Finland under the Finnish Centre of Excellence Programme 2012–2017 (Nuclear and Accelerator Based Physics Research at JYFL) and Projects No. 306980, No. 312544, No. 275389, No. 284516, No. 295207, No. 314733, No. 315179, No. 327629, No. 320062, No. 354589, and No. 345869. The support by the EU Horizon 2020 research and innovation program under Grant no. 771036 (ERC CoG MAIDEN) is acknowledged. This project has received funding from the European Union's Horizon 2020 research and innovation programme under Grant Agreement No. 861198–LISA–H2020-MSCA-ITN-2019.

[1] Y. Fukuda, T. Hayakawa, E. Ichihara, K. Inoue, K. Ishihara, H. Ishino, Y. Itow, T. Kajita, J. Kameda, S. Kasuga *et al.*, Phys. Rev. Lett. **81**, 1562 (1998).
[2] Q. R. Ahmad, R. C. Allen, T. C. Andersen, J. D. Anglin, J. C. Barton, E. W. Beier, M. Bercovitch, J. Bigu, S. D. Biller, R. A. Black, I. Blevis *et al.*, Phys. Rev. Lett. **89**, 011301 (2002).
[3] M. Gerbino and M. Lattanzi, Front. Phys. **5**, 70 (2018).
[4] J. Suhonen and O. Civitarese, Phys. Rep. **300**, 123 (1998).
[5] F. T. Avignone, S. R. Elliott, and J. Engel, Rev. Mod. Phys. **80**, 481 (2008).
[6] H. Ejiri, J. Suhonen, and K. Zuber, Phys. Rep. **797**, 1 (2019).
[7] M. Aker, A. Beglarian, J. Behrens, A. Berlev, U. Besserer, B. Bieringer, F. Block, B. Bornschein, L. Bornschein, M. Böttcher *et al.*, Nat. Phys. **18**, 160 (2022).
[8] C. Velte, F. Ahrens, A. Barth, K. Blaum, M. Braß, M. Door, H. Dorrer, C. E. Düllmann, S. Eliseev, C. Enss *et al.*, Eur. Phys. J. C **79**, 1026 (2019).
[9] A. B. McDonald, G. Drexlin, V. Hannen, S. Mertens, and C. Weinheimer, Adv. High Energy Phys. **2013**, 293986 (2013).
[10] E. Ferri, D. Bagliani, M. Biasotti, G. Ceruti, D. Corsini, M. Faverzani, F. Gatti, A. Giachero, C. Gotti, C. Kilbourne, A. Kling, M. Maino, P. Manfrinetti, A. Nucciotti, G. Pessina, G. Pizzigoni, M. Ribeiro Gomes, and M. Sisti, Phys. Proc. **61**, 227 (2015).

[11] Z. Ge, T. Eronen, A. de Roubin, K. Tyrin, L. Canete, S. Geldhof, A. Jokinen, A. Kankainen, J. Kostensalo, J. Kotila *et al.*, Phys. Lett. B **832**, 137226 (2022).

[12] Z. Ge, T. Eronen, K. S. Tyrin, J. Kotila, J. Kostensalo, D. A. Nesterenko, O. Beliuskina, R. de Groote, A. de Roubin *et al.*, Phys. Rev. Lett. **127**, 272301 (2021).

[13] E. G. Myers, A. Wagner, H. Kracke, and B. A. Wesson, Phys. Rev. Lett. **114**, 013003 (2015).

[14] M. Redshaw, Eur. Phys. J. A **59**, 18 (2023).

[15] M. Haaranen and J. Suhonen, Eur. Phys. J. A **49**, 93 (2013).

[16] J. Suhonen, Phys. Scr. **89**, 054032 (2014).

[17] R. Sandler, G. Bollen, N. D. Gamage, A. Hamaker, C. Izzo, D. Puentes, M. Redshaw, R. Ringle, and I. Yandow, Phys. Rev. C **100**, 024309 (2019).

[18] J. Karthein, D. Atanasov, K. Blaum, S. Eliseev, P. Filianin, D. Lunney, V. Manea, M. Mougeot, D. Neidherr, Y. Novikov *et al.*, Hyperfine Interact. **240**, 61 (2019).

[19] A. De Roubin, J. Kostensalo, T. Eronen, L. Canete, R. P. De Groote, A. Jokinen, A. Kankainen, D. A. Nesterenko, I. D. Moore *et al.*, Phys. Rev. Lett. **124**, 222503 (2020).

[20] Z. Ge, T. Eronen, A. de Roubin, D. A. Nesterenko, M. Hukkanen, O. Beliuskina, R. de Groote, S. Geldhof, W. Gins, A. Kankainen *et al.*, Phys. Rev. C **103**, 065502 (2021).

[21] T. Eronen, Z. Ge, A. de Roubin, M. Ramalho, J. Kostensalo, J. Kotila, O. Beliushkina, C. Delafosse, S. Geldhof, W. Gins *et al.*, Phys. Lett. B **830**, 137135 (2022).

[22] Z. Ge, T. Eronen, A. de Roubin, J. Kostensalo, J. Suhonen, D. A. Nesterenko, O. Beliuskina, R. de Groote, C. Delafosse, S. Geldhof *et al.*, Phys. Rev. C **106**, 015502 (2022).

[23] M. Ramalho, Z. Ge, T. Eronen, D. A. Nesterenko, J. Jaatinen, A. Jokinen, A. Kankainen, J. Kostensalo, J. Kotila, M. I. Krivoruchenko *et al.*, Phys. Rev. C **106**, 015501 (2022).

[24] D. K. Keblbeck, R. Bhandari, N. D. Gamage, M. Horana Gamage, K. G. Leach, X. Mougeot, and M. Redshaw, Phys. Rev. C **107**, 015504 (2023).

[25] L. Gastaldo, J. Low Temp. Phys. **209**, 804 (2022).

[26] C. L. Longmire, Phys. Rev. **75**, 15 (1949).

[27] M. Pfützner, K. Pachucki, and J. Żylicz, Phys. Rev. C **92**, 044305 (2015).

[28] S. Haselschwardt, B. Lenardo, P. Pirinen, and J. Suhonen, Phys. Rev. D **102**, 072009 (2020).

[29] M. M. Al-Hamidi, A. M. Demidov, M. M. Dyufani, M. S. El-Ahrash, I. V. Mikhailov, D. M. Rateb, S. M. Sergiwa, A. M. Shermit, and S. M. Zlitni, Yad. Fiz. **57**, 545 (1994).

[30] S. Mukhopadhyay, M. Scheck, B. Crider, S. N. Choudry, E. Elhami, E. Peters, M. T. McEllistrem, J. N. Orce, and S. W. Yates, Phys. Rev. C **78**, 034317 (2008).

[31] I. Dioszegi, C. Maraczy, and A. Veres, Nucl. Phys. A **438**, 395 (1985).

[32] National Nuclear Data Center, available at https://www.nndc.bnl.gov/ (2020/4/7).

[33] M. Wang, W. Huang, F. Kondev, G. Audi, and S. Naimi, Chin. Phys. C **45**, 030003 (2021).

[34] J. L. Olsen and G. D. O'Kelley, Phys. Rev. **95**, 1539 (1954).

[35] R. Reising and B. Pate, Nucl. Phys. **65**, 609 (1965).

[36] D. Fink, J. Barea, D. Beck, K. Blaum, C. Böhm, C. Borgmann, M. Breitenfeldt, F. Herfurth, A. Herlert, J. Kotila *et al.*, Phys. Rev. Lett. **108**, 062502 (2012).

[37] D. A. Nesterenko, L. Canete, T. Eronen, A. Jokinen, A. Kankainen, Y. N. Novikov, S. Rinta-Antila, A. de Roubin, and M. Vilen, Int. J. Mass Spectrom. **435**, 204 (2019).

[38] I. D. Moore, T. Eronen, D. Gorelov, J. Hakala, A. Jokinen, A. Kankainen, V. S. Kolhinen, J. Koponen, H. Penttilä, and I. Pohjalainen, Nucl. Instrum. Methods Phys. Res. B **317**, 208 (2013).

[39] T. Eronen, V. S. Kolhinen, V. V. Elomaa *et al.*, Eur. Phys. J. A **48**, 46 (2012).

[40] P. Karvonen, I. D. Moore, T. Sonoda, T. Kessler, H. Penttilä, K. Peräjärvi, P. Ronkanen, and J. Äystö, Nucl. Instrum. Methods Phys. Res. B **266**, 4794 (2008).

[41] A. Nieminen, J. Huikari, A. Jokinen, J. Äystö, P. Campbell, and E. C. Cochrane, Nucl. Instrum. Methods Phys. Res. A **469**, 244 (2001).

[42] T. Eronen, V. V. Elomaa, U. Hager, J. Hakala, A. Jokinen, A. Kankainen, S. Rahaman, J. Rissanen, C. Weber, and J. Äystö, Acta Phys. Pol. B **39**, 445 (2008).

[43] D. A. Nesterenko, T. Eronen, A. Kankainen, L. Canete, A. Jokinen, I. D. Moore, H. Penttilä, S. Rinta-Antila, A. de Roubin, and M. Vilen, Eur. Phys. J. A **54**, 154 (2018).

[44] D. A. Nesterenko, T. Eronen, Z. Ge, A. Kankainen, and M. Vilen, Eur. Phys. J. A **57**, 302 (2021).

[45] G. Savard, S. Becker, G. Bollen, H. J. Kluge, R. B. Moore, T. Otto, L. Schweikhard, H. Stolzenberg, and U. Wiess, Phys. Lett. A **158**, 247 (1991).

[46] S. Eliseev, K. Blaum, M. Block, A. Dörr, C. Droese, T. Eronen, M. Goncharov, M. Höcker, J. Ketter, E. M. Ramirez, D. A. Nesterenko, Y. N. Novikov, and L. Schweikhard, Appl. Phys. B **114**, 107 (2014).

[47] S. Eliseev, K. Blaum, M. Block, C. Droese, M. Goncharov, E. Minaya Ramirez, D. A. Nesterenko, Y. N. Novikov, and L. Schweikhard, Phys. Rev. Lett. **110**, 082501 (2013).

[48] A. Kramida, Yu. Ralchenko, J. Reader, and NIST ASD Team, NIST Atomic Spectra Database (ver. 5.8), available online at `https://physics.nist.gov/asd` [2021, January 19], National Institute of Standards and Technology, Gaithersburg, MD (2020).

[49] A. Kellerbauer, K. Blaum, G. Bollen, F. Herfurth, H. J. Kluge, M. Kuckein, E. Sauvan, C. Scheidenberger, and L. Schweikhard, Euro. Phys. J. D **22**, 53 (2003).

[50] C. Roux, K. Blaum, M. Block, C. Droese, S. Eliseev, M. Goncharov, F. Herfurth, E. M. Ramirez, D. A. Nesterenko, Y. N. Novikov, and L. Schweikhard, Eur. Phys. J. D **67**, 146 (2013).

[51] R. T. Birge, Phys. Rev. **40**, 207 (1932).

[52] W. Huang, M. Wang, F. Kondev, G. Audi, and S. Naimi, Chin. Phys. C **45**, 030002 (2021).

[53] B. A. Brown, N. J. Stone, J. R. Stone, I. S. Towner, and M. Hjorth-Jensen, Phys. Rev. C **71**, 044317 (2005).

[54] B. Brown and W. Rae, Nucl. Data Sheets **120**, 115 (2014).

[55] J. T. Suhonen, Front. Phys. **5**, 55 (2017).

[56] J. Kotila and F. Iachello, Phys. Rev. C **85**, 034316 (2012).

[57] N. Gove and M. Martin, At. Data Nucl. Data Tables **10**, 205 (1971).

[58] R. Davis, D. S. Harmer, and K. C. Hoffman, Phys. Rev. Lett. **20**, 1205 (1968).

[59] R. S. Raghavan, Phys. Rev. Lett. **78**, 3618 (1997).

[60] S. J. Haselschwardt, B. G. Lenardo, T. Daniels, S. W. Finch, F. Q. L. Friesen, C. R. Howell, C. R. Malone, E. Mancil, and W. Tornow, Phys. Rev. Lett. **131**, 052502 (2023).

[61] J. L. Newstead, L. E. Strigari, and R. F. Lang, Phys. Rev. D **99**, 043006 (2019).
[62] S. Appel, Z. Bagdasarian, D. Basilico, G. Bellini, J. Benziger, R. Biondi, B. Caccianiga, F. Calaprice, A. Caminata, P. Cavalcante *et al.*, Phys. Rev. Lett. **129**, 252701 (2022).
[63] J. N. Bahcall, Phys. Rev. D **49**, 3923 (1994).
[64] M. Redshaw, E. Wingfield, J. McDaniel, and E. G. Myers, Phys. Rev. Lett. **98**, 053003 (2007).
[65] J. A. Dror, G. Elor, and R. McGehee, Phys. Rev. Lett. **124**, 181301 (2020).